ACS Photonics

Letter

pubs.acs.org/journal/apchd5

Electrically Controllable Light Trapping for Self-Powered Switchable Solar Windows

Joseph Murray,[†,‡] Dakang Ma,[†,‡] and Jeremy N. Munday*[,†,‡]

[†]Department of Electrical and Computer Engineering, University of Maryland, College Park, Maryland 20742, United States

[‡]Institute for Research in Electronics and Applied Physics, University of Maryland, College Park, Maryland 20740, United States

Supporting Information

ABSTRACT: The ability to electrically control transparency and scattering of light is important for many optoelectronic devices; however, such versatility usually comes with additional unwanted optical absorption and power loss. Here we present a hybrid switchable solar window device based on polymer dispersed liquid crystals (PDLCs) coupled to a semiconducting absorber, which can switch between highly transmissive and highly scattering states while simultaneously generating power. By applying a voltage across the PDLC layer, the device switches from an opaque, light-scattering structure (useful for room light dimming, privacy, and temperature control) to a clear, transparent window. Further, enabled by the very low operating power requirements of the PDLC (<0.8 mW/cm^2), we demonstrate that these switchable solar windows have the potential for self-powering with as little as 13 nm of a-Si.

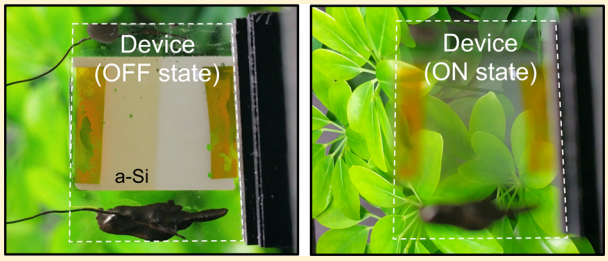

KEYWORDS: *photovoltaics, smart window, liquid crystal, light trapping*

In order to absorb a significant fraction of the incident solar irradiation, thin-film photovoltaic devices require light trapping and scattering.[1−7] However, for some applications, such as building-integrated photovoltaics (BIPV),[8−22] partial absorption is preferred to enable operation as a semitransparent window. The basic trade-off between power generation and window transparency must be decided *a priori*. An alternative technology, switchable smart windows, has recently gained considerable interest for both privacy and climate control,[23] and these smart windows have been designed to modulate their optical transmission using a wide range of mechanisms including electrochromism,[15,23−27] thermochromism,[20,28−30] and liquid crystal alignment.[14,23,26,31−34] These devices often target control of sunlight to reduce heating and cooling loads or to enhance user comfort by modifying the intensity/spectrum of solar irradiance entering the building.[23,24,35] Some smart windows have demonstrated mechanical self-powering or automatic response to changing conditions[25,27,34,36,37] using photovoltaics or a chemical process that responds to light or heat. However, they work by modifying the absorptivity of the switching material, which results in wasted energy from the incident light.

Here we present a self-powered switchable smart window concept that enables variable transmissivity, diffusivity, and power generation on-demand that can be adjusted throughout the day. The design consists of a thin absorbing layer (a-Si) and an actively tunable scattering material (polymer-dispersed liquid crystal) that allows the device to switch between a low-power-generating transparent state (1.9 mW/cm^2) and a high-power-generating diffuse state (3.2 mW/cm^2) for a 28 nm a-Si film. The power required to operate the device is <0.8 mW/cm^2, showing that under typical solar illumination it is self-powering.

To switch between a transparent and diffuse state, the device incorporates a polymer-dispersed liquid crystal (PDLC) layer (Figure 1), which is composed of microdroplets of a liquid crystal (LC) material dispersed in a polymer matrix. As expected, in its OFF state (no applied voltage), PDLCs strongly scatter light, appearing hazy or opaque due to light scattering from the random orientation of the liquid crystals, resulting in refractive index variation throughout the material. When enough voltage is applied across the film, the liquid crystal alignment reduces the refractive index contrast for light traveling parallel to the alignment direction, and the material becomes highly transparent owing to the suppressed scattering.[38] Since its original discovery,[39] researchers have extensively explored the potential applications of PDLCs in the areas of flat panel displays,[40,41] smart windows,[26,42] and microlenses.[43] Nematic liquid crystals are the most common type employed in PDLC devices. The droplets are optically birefringent with ordinary refractive index n_o along two optical axes and extraordinary refractive index n_e along the third axis. The polymer is optically isotropic with refractive index n_p. In the absence of an applied electric field (OFF state), the optical axes of individual droplets align approximately randomly, resulting in spatial variations of refractive index across the film, which cause strong light scattering. In the presence of an

Received: July 22, 2016
Published: October 26, 2016

DOI: 10.1021/acsphotonics.6b00518
ACS Photonics 2017, 4, 1−7

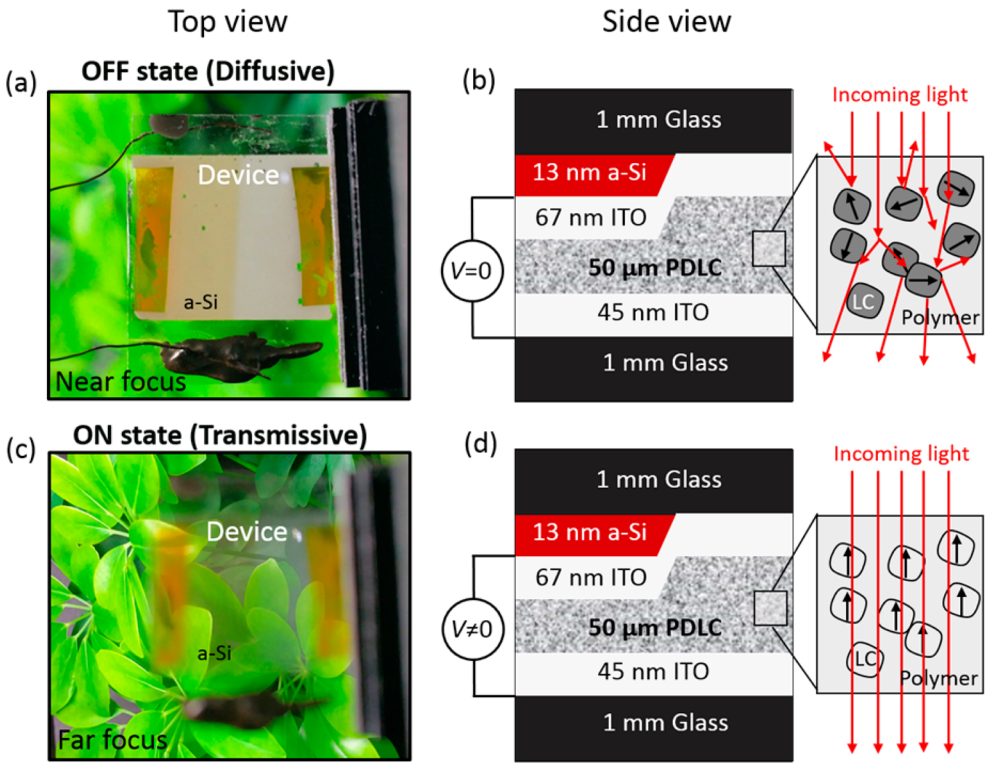

Figure 1. (a) Photograph and (b) schematic of a representative device in the OFF (i.e., diffusive) state with no applied bias. The structure is 2.00 cm × 1.57 cm, and the plant in the background is held at a distance of 35 cm. The amber-colored side of the device (left) incorporates a 13 nm a-Si layer, while the right side has no additional absorbing layer for comparison. In the OFF state, the liquid crystal microdroplets are randomly oriented. The refractive index variation causes significant light scattering, which results in diffuse transmission, and hence can be used as a privacy window. (c) Photograph and (d) schematic of the same device in the ON (i.e., transmissive) state with an applied voltage of 150 V (square wave). The liquid crystal alignment in the ON state results in a uniform refractive index for normally incident light and, thus, high transmission.

electric field (ON state), molecules in a liquid crystal material with positive dielectric anisotropy align their long axes parallel to the applied electric field. In this case, light incident normal to the plane of the film experiences a refractive index of n_o in the liquid crystal droplets. When n_o and n_p are matched, the film is transparent in this state.[44] Smart widows incorporating PDLCs can use the dynamic opacity variation for privacy, for glare reduction, and to minimize the cost of indoor climate control;[14,23,26] however, to remain in a transparent state, power must be continuously supplied to the window at relatively high voltages (10−150 V depending on the thickness and materials used[23,45]). Note that the transparency switching of PDLC devices is particularly useful when compared to other liquid crystal technologies that use polarizers, because it switches between reflective and scattering (rather than absorptive), which reduces optical energy loss.

To create a self-powered switchable smart window, we combine a PDLC cell with an a-Si absorbing layer. In the ON state of the PDLC, the cell is highly transparent, and in the OFF state the absorption in the a-Si is enhanced by the scattering from the PDLC. We use previously developed techniques to accurately determine the absorption in the a-Si layer[46,47] and demonstrate that a complete photovoltaic device would achieve self-powering even in the weakly absorbing ON state. In contrast to other switchable smart window devices that modulate transmission by increasing absorption, these PDLC-based devices modulate transmission via scattering. The reflective scattering while in the OFF state captures this otherwise wasted energy and significantly increases photovoltaic performance. Further we show that these devices have several favorable characteristics for privacy and temperature control, such as switchablilty of haze, opacity, and overall transmission.

Figure 1 shows the device operation and a schematic of both the transparent and opaque states (see Video 1 in the SI). The structures consist of an E7 liquid crystal suspended in NOA65 optical adhesive sandwiched between indium tin oxide (ITO)-coated glass slides. Each device contains a 13 nm thick layer of a-Si, which covers half the structure (Figure 1b). Here we chose a-Si because it is a common thin-film solar cell material for which we can easily control the deposition thickness (see Methods section for details about sample preparation). However, note that no attempt is made in this demonstration to dope these very thin a-Si layers, as they are used primarily as an example absorber. For the OFF state of the device, no voltage is applied between the top and bottom ITO layers. In the ON state, a 200 Hz square wave is applied between the leads (note: dc operation for extended amounts of time can damage PDLC layers due to ion migration[48]). While the devices are capable of continuous variation of opacity, for simplicity and clarity, we chose binary operation at either 0 V (OFF, diffusive) or 150 V (ON, transmissive).

Devices are fabricated and tested with different a-Si layer thicknesses (13 and 28 nm) to determine the optical properties in both the ON and OFF states. Absorption (and transmission) measurements are made using chopped monochromatic illumination with an integrating sphere, to capture scattered light. The sphere incorporates a silicon photodiode monitored by a lock-in amplifier for readout (see SI for details). Figure 2a−d shows the total absorption both measured (circles) and

DOI: 10.1021/acsphotonics.6b00518
ACS Photonics 2017, 4, 1−7

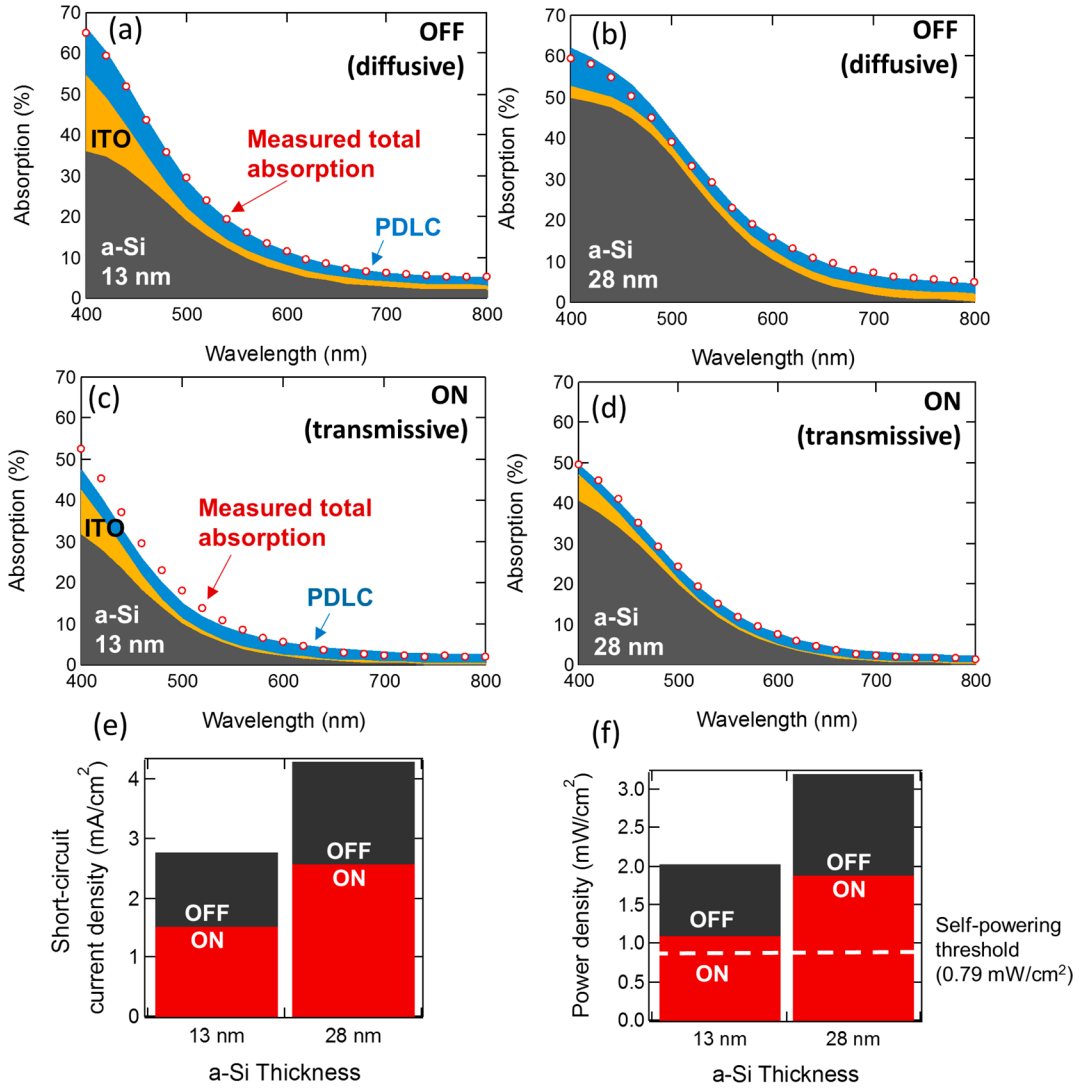

Figure 2. (a–d) Measured (circles) and calculated (shaded areas) absorption for devices with two a-Si thicknesses (13 nm (a, c) and 28 nm (b, d)) in the OFF state (a, b) and the ON state (c, d). The absorption is calculated in each material, and the total absorption is measured. Calculated (e) short-circuit current density and (f) power generation density are shown with the self-powering threshold marked as a dashed line.

calculated (solid lines), as well as the absorption in individual layers (represented by the colored areas). Note that the data for both ITO layers (top and bottom) are combined in this plot. The absorption in the individual layers is calculated by determining the total electric field power density in each layer (adding reflections/transmissions from thin films coherently) and using the absorption coefficient for each material (see SI). In the OFF (i.e., diffusive) state, the data are calculated following ref 47 under the assumption that light entering the PDLC becomes fully randomized, which is supported by internal scattering measurements[47] (see SI). ON state calculations assume no scattering. The total measured and calculated data are in close agreement with RMS errors of 0.43%, 1.3%, 2.4%, and 0.48% (absolute) for the data in Figure 2a–d, respectively.

After determining the total absorption within the a-Si layer, we calculate the expected power generation from a complete photovoltaic cell incorporated into the switchable solar window and determine the potential for self-powering. While developing a high-performance a-Si solar cell is beyond the scope of this work, we calculate short-circuit current density based on the measured absorption within the a-Si layer of the PDLC device (Figure 2a–d), weighted by the AM1.5G solar spectrum. The short-circuit current density is used to determine the generated power density (Figure 2f) using a single diode model, where the reverse saturation current is obtained by extrapolation from experimental data of a high-quality a-Si solar cell[49,50] (see SI). The dotted line in Figure 2f indicates the threshold for self-powering, given by the power consumption of the PDLC device in the ON state divided by the area of the cell (3.14 cm^2), as described below.

The measured power consumption within the PDLC layer is determined in two steps because of the large dynamic range required for the measurement (~6 orders of magnitude); see Figure 3. First, the power is measured during the charging and discharging of the PDLC (driven by a square wave at 200 Hz) due to its capacitance. Second, the power is measured during steady-state current operation, which is found to be 3.5 μA, corresponding to a shunt resistance of 42 MΩ. Figure 3a shows the voltage applied across the device as a function of time, and Figure 3b,c shows a zoom-in of the voltage, current, and power used during a polarity switching event (shaded region in Figure

DOI: 10.1021/acsphotonics.6b00518
ACS Photonics 2017, 4, 1–7

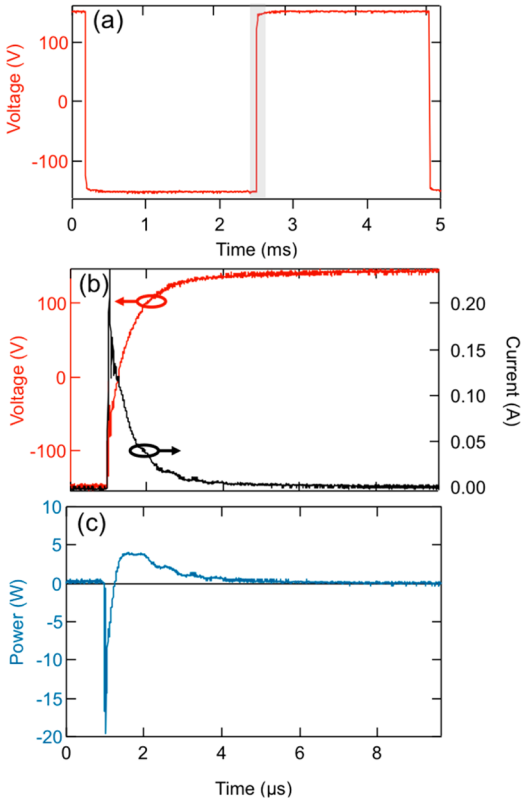

Figure 3. Electrical characteristics of the PDLC switchable self-powered solar window. (a) Voltage across the device as a function of time during operation in the ON state (applied square wave function with voltage of 150 V). The gray region near 2.5 ms is expanded in (b) and (c) for clarity. Measured (b) voltage, current, and (c) power consumed by the device during a polarity switching event. Negative power usage regions correspond to the recovery of energy stored via the capacitive nature of the device. The total power density needed for device operation is <0.8 mW/cm^2.

3a). Here, the negative power corresponds to the energy recovered by discharging the PDLC cell. The total average power density needed to operate the device is <0.8 mW/cm^2, comparable to commercially available ones.[23] In all cases considered here, this power requirement can be met by the solar energy potentially converted by the a-Si absorbing layer. Further, the OFF state of the device with the 28 nm a-Si layer generates nearly 4 times the needed power, and the OFF state of the 13 nm a-Si layer device creates more than 2.5 times the required power.

The generated power can be increased using a thicker absorbing a-Si layer; however, there is a decrease in transmission, as shown in Figure 4a. The structure with no a-Si (corresponding to maximum transmission but no power generation) has a nearly flat, colorless transmission spectrum with a 13% change between 460 and 650 nm (the range over which the photopic sensitivity of the human eye is >10% of the maximum sensitivity[51]). For the device with a 13 nm a-Si layer, we observe a similar flatness for $\lambda \geq 500$ nm, resulting in a slight amber or brown tint (Figure 1a,c). For the device with a 28 nm a-Si layer, we observe the same trend but with a slightly darker tint. While not completely colorless, they do demonstrate the generally accepted light brown color for tinted glass. The transmission in the OFF state shows the same trends but at a lower mean value (Figure 4a) due to the increased reflection and scattering, which benefits the power generation (Figure 2). In the wavelength range shown, the AM1.5G weighted transmission can be reduced by more than a third by switching between the ON and OFF states. The luminous transmittance (CIE 1931 human perception of transmittance) for an AM1.5G spectrum is 74%, 68%, and 65%, respectively, for devices with no a-Si, 13 nm a-Si, and 28 nm a-Si in the ON state and is 45%, 41%, and 40% in the OFF state, respectively (see SI for details on chromaticity). In contrast to many other smart window designs, this reduction is primarily due to reflection rather than absorption, which can have a very significant impact on cooling costs by limiting optical heating of the windowed room.[23,24,35]

In addition to the nearly flat transmission spectrum, the device scatters light uniformly in all directions when operating in the OFF state, demonstrating its effectiveness as a privacy window. Figure 4b shows a polar plot of the scattered transmission and reflection as a function of wavelength for a typical PDLC device with no a-Si in the OFF state (normalized to the near-normal incidence reflection data). The optical scattering is characterized by monochromatic illumination on the device using a custom-built goniometer (see Methods section and SI for details). Note that these data are obtained from a more complete scattering characterization that includes internal scattering within the device (see SI), where a nearly Lambertian scattering profile is found for all wavelengths.

For window applications, device performance at oblique incidence is important. Figure 5 shows the measured absorption in both the ON and OFF states for the structure

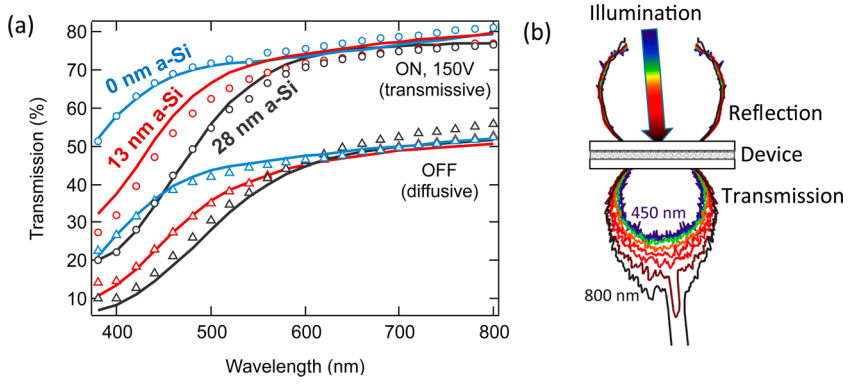

Figure 4. (a) Transmission spectra for the PDLC switchable solar windows in the ON (circles) and OFF (triangles) states. The solid lines refer to the modeled transmission. (b) Polar plot of the scattered transmission and reflection as a function of wavelength for the device in the OFF state.

DOI: 10.1021/acsphotonics.6b00518
ACS Photonics 2017, 4, 1−7

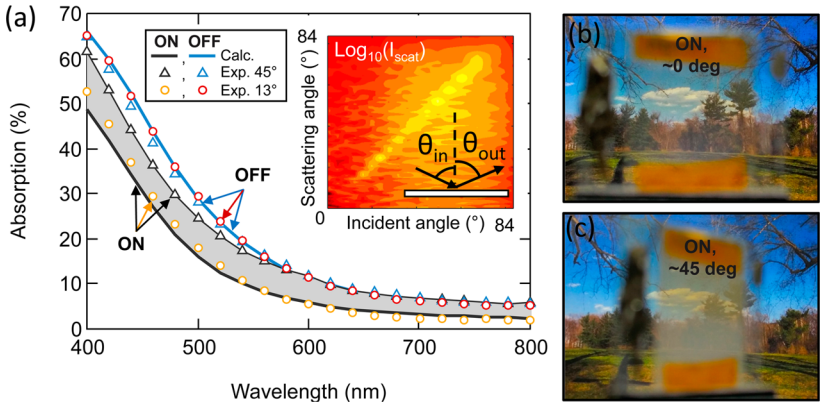

Figure 5. (a) Measured (open symbols) and calculated (solid lines) absorption for the PDLC device with 13 nm of a-Si. Here, the absorption at a 45° incident angle is compared to the near-normal absorption from Figure 2. The shaded region denotes the difference between the measured ON state absorption at 45° illumination and the calculated ON state absorption at 45° illumination assuming no scattering. The inset shows a log map of scattered light intensity as a function of both incident (θ_{in}) and reflected scattering (θ_{out}) angles. Optical image through the device in the ON state at (b) normal incidence and (c) 45° from normal (see also Video 2 of the SI).

with 13 nm thick a-Si at both near-normal incidence and 45-degree illumination. The absorption in the OFF state is very weakly affected by the change in angle. However, the measured absorption in the ON state is markedly different at 45°, and it is significantly greater than the calculated value. This difference is explained by the inset of Figure 5, which shows the scattered intensity as a function of both incident and scattered angles. At near-normal incidence, almost no scattering occurs. As the incident angle increases to 45°, scattering increases with most light scattered at large angles. This behavior is due to the random position of the liquid crystal microdroplets. Though the applied field in the ON state orients the optical axis of the microdroplets, light entering at non-normal incidence has a component traveling along the extraordinary axis of the liquid crystal, which is scattered by the index contrast with the polymer. This effect can have a large influence on absorption because light is preferentially scattered at larger angles due to the higher index for light traveling in that direction (for in-depth details on scattering see refs 46, 47, and 52). Note that the scattering in the ON state is still weaker than in the OFF state (see SI for details of OFF state scattering and internal scattering distributions). The measured absorption in the OFF state for 45-degree illumination would yield 1.3 mW/cm^2 of power generation, which is greater than the self-powering threshold, thus demonstrating that these devices would be self-powering. For the ON state at 45-degree illumination, the absorption within the a-Si is expected to be at least as high as in the near-normal case, based on the higher measured absorption compared to the model. Thus, a minimum power generation of >0.8 mW/cm^2 is expected, again enabling self-powering.

In conclusion, we have presented smart, switchable solar window devices based on an a-Si absorber and a PLDC transmission modulator. We demonstrated that these devices have the potential to self-power even in the low absorption state with as little as 13 nm of a-Si and have excellent smart window properties: high transparency and clarity (ON state) and high diffusivity (OFF state) for enhanced privacy and reduced solar heating. Their performance is further improved for non-normal incident illumination, which is typical for real-world deployment in building integrated PV applications. These characteristics demonstrate the great potential of these switchable solar window devices with actively tunable power generation and transparency control.

METHODS

Sample Preparation. The bottom ITO-coated glass was obtained from a commercial manufacturer (SPI part #6466-AB). The a-Si layer was deposited by RF sputtering in argon onto glass coverslips. Samples were mechanically shadowed, covering only half of the glass with absorbing a-Si (Figure 1). This shadowing procedure allowed for later direct measurement of the PDLC cell on the same device without a-Si. The absorbing layer was then coated with ITO by sputtering from a single ITO target in 7% oxygen, 93% argon. During each sputtering step, additional samples were included for later characterization (see below). The PDLC mixture consisted of liquid crystal E7 and photocurable polymer NOA65 (Norland Products) with 50:50 weight ratio. It was then filled into an empty cell made with the top and bottom coated glass slides, separated by a Kapton spacer layer approximately 50 μm thick. The cell was then cured at room temperature for 1 min with a UV lamp.[53]

Material Characterization. The materials were characterized using ellipsometry, atomic force microscopy (AFM), and absorption and transmission measurements. The refractive indices of the films were measured by ellipsometry. Film thicknesses and roughnesses (found to be negligible at <5 Å RMS for the a-Si films and 7 Å RMS for the ITO film) were measured by AFM and confirmed with ellipsometry (see SI). The imaginary part of the index of refraction was further refined (ellipsometry was relatively insensitive to very small amounts of absorption) by adjusting the ellipsometric fit to jointly agree with the independent absorption measurements. Absorption and transmission were measured in a 6 in. integrating sphere (Labsphere RTC-060). This sphere uses a center mounting holder for direct measurement of absorption (from the total combined reflection and transmission). Absorption was measured at 13° incidence for near-normal measurements, while transmission was measured at 7° incidence (difference due to geometric requirements of the system). The integrating sphere light intensity was monitored by a Si photodiode, and this signal was used by a lock-in amplifier. The light source was a Xe lamp followed by a monochromator (SPEX 500M). Incident power was monitored to account for variations in the incident intensity, and second-order diffuse absorption in the sample (light reflected or

DOI: 10.1021/acsphotonics.6b00518
ACS Photonics 2017, 4, 1−7

transmitted from the sample and absorbed after scattering from the integrating sphere) was accounted for by illuminating the sphere through a secondary port for calibration.

The internal scattering distribution (angularly resolved scattering inside the sample layers) was determined for accurate absorption calculations using a gonioreflectometer and by replacing the glass slide on one side with a glass hemisphere, as described in ref 47. The OFF state per pass absorption and transmission was characterized by measurements on the part of the sample without a-Si.

To determine the power dissipated within the device, the current was measured by the voltage drop across a 1.2 kΩ current sensing resistor, and the voltage across the device was measured directly. These time-dependent measurements were made using an oscilloscope.

■ ASSOCIATED CONTENT

Supporting Information

The Supporting Information is available free of charge on the ACS Publications website at DOI: 10.1021/acsphotonics.6b00518.

Details on device characterization and power density calculations (PDF)

Videos of device operation (ZIP)

■ AUTHOR INFORMATION

Corresponding Author

*E-mail: jnmunday@umd.edu.

Author Contributions

J.N.M. and J.M. conceived the project. J.M. performed the experiments and the calculations. D.M. prepared samples. J.N.M. supervised this project. All authors contributed to the manuscript.

Notes

The authors declare no competing financial interest.

■ ACKNOWLEDGMENTS

Authors acknowledge the University of Maryland and its Fab Lab, as well as M. S. Leite for helpful comments and suggestions. Partial support for this project was from a NASA Early Career Faculty Award (No. NNX12AQ50G) and NASA Smallsat Patnership Award (No. NNX15AW53A).

■ REFERENCES

(1) Ferry, V. E.; Munday, J. N.; Atwater, H. A. Design Considerations for Plasmonic Photovoltaics. *Adv. Mater.* **2010**, *22*, 4794−4808.

(2) Brongersma, M. L.; Cui, Y.; Fan, S. Light Management for Photovoltaics Using High-Index Nanostructures. *Nat. Mater.* **2014**, *13*, 451−460.

(3) Callahan, D. M.; Munday, J. N.; Atwater, H. A. Solar Cell Light Trapping beyond the Ray Optic Limit. *Nano Lett.* **2012**, *12*, 214−218.

(4) Catchpole, K. R.; Polman, A. Design Principles for Particle Plasmon Enhanced Solar Cells. *Appl. Phys. Lett.* **2008**, *93*, 191113.

(5) Yu, Z.; Raman, A.; Fan, S. Thermodynamic Upper Bound on Broadband Light Coupling with Photonic Structures. *Phys. Rev. Lett.* **2012**, *109*, 173901.

(6) Yu, Z.; Raman, A.; Fan, S. Fundamental Limit of Light Trapping in Grating Structures. *Opt. Express* **2010**, *18*, A366−A380.

(7) Rau, U.; Paetzold, U. W.; Kirchartz, T. Thermodynamics of Light Management in Photovoltaic Devices. *Phys. Rev. B: Condens. Matter Mater. Phys.* **2014**, *90*, 35211.

(8) Chen, C.-C.; Dou, L.; Zhu, R.; Chung, C.-H.; Song, T.-B.; Zheng, Y. B.; Hawks, S.; Li, G.; Weiss, P. S.; Yang, Y. Visibly Transparent Polymer Solar Cells Produced by Solution Processing. *ACS Nano* **2012**, *6*, 7185−7190.

(9) Betancur, R.; Romero-Gomez, P.; Martinez-Otero, A.; Elias, X.; Maymó, M.; Martorell, J. Transparent Polymer Solar Cells Employing a Layered Light-Trapping Architecture. *Nat. Photonics* **2013**, *7*, 995−1000.

(10) Zhang, H.; Jenatsch, S.; De Jonghe, J.; Nüesch, F.; Steim, R.; Véron, A. C.; Hany, R. Transparent Organic Photodetector Using a Near-Infrared Absorbing Cyanine Dye. *Sci. Rep.* **2015**, *5*, 9439.

(11) Zhao, Y.; Lunt, R. R. Transparent Luminescent Solar Concentrators for Large-Area Solar Windows Enabled by Massive Stokes-Shift Nanocluster Phosphors. *Adv. Energy Mater.* **2013**, *3*, 1143−1148.

(12) Zhao, Y.; Meek, G. A.; Levine, B. G.; Lunt, R. R. Near-Infrared Harvesting Transparent Luminescent Solar Concentrators. *Adv. Opt. Mater.* **2014**, *2*, 606−611.

(13) Debije, M. G. Solar Energy Collectors with Tunable Transmission. *Adv. Funct. Mater.* **2010**, *20*, 1498−1502.

(14) Khandelwal, H.; Loonen, R. C. G. M.; Hensen, J. L. M.; Debije, M. G.; Schenning, A. P. H. J. Electrically Switchable Polymer Stabilised Broadband Infrared Reflectors and Their Potential as Smart Windows for Energy Saving in Buildings. *Sci. Rep.* **2015**, *5*, 11773.

(15) Ahn, K.-S.; Yoo, S. J.; Kang, M.-S.; Lee, J.-W.; Sung, Y.-E. Tandem Dye-Sensitized Solar Cell-Powered Electrochromic Devices for the Photovoltaic-Powered Smart Window. *J. Power Sources* **2007**, *168*, 533−536.

(16) Ameri, T.; Dennler, G.; Waldauf, C.; Azimi, H.; Seemann, A.; Forberich, K.; Hauch, J.; Scharber, M.; Hingerl, K.; Brabec, C. J. Fabrication, Optical Modeling, and Color Characterization of Semitransparent Bulk-Heterojunction Organic Solar Cells in an Inverted Structure. *Adv. Funct. Mater.* **2010**, *20*, 1592−1598.

(17) Guo, F.; Ameri, T.; Forberich, K.; Brabec, C. J. Semitransparent Polymer Solar Cells. *Polym. Int.* **2013**, *62*, 1408−1412.

(18) Chen, K.-S.; Salinas, J.-F.; Yip, H.-L.; Huo, L.; Hou, J.; Jen, A. K.-Y. Semi-Transparent Polymer Solar Cells with 6% PCE, 25% Average Visible Transmittance and a Color Rendering Index close to 100 for Power Generating Window Applications. *Energy Environ. Sci.* **2012**, *5*, 9551−9557.

(19) Eperon, G. E.; Burlakov, V. M.; Goriely, A.; Snaith, H. J. Neutral Color Semitransparent Microstructured Perovskite Solar Cells. *ACS Nano* **2014**, *8*, 591−598.

(20) Guo, F.; Chen, S.; Chen, Z.; Luo, H.; Gao, Y.; Przybilla, T.; Spiecker, E.; Osvet, A.; Forberich, K.; Brabec, C. J. Printed Smart Photovoltaic Window Integrated with an Energy-Saving Thermochromic Layer. *Adv. Opt. Mater.* **2015**, *3*, 1524−1529.

(21) Jin, H.; Qian, J.; Zhou, L.; Yuan, J.; Huang, H.; Wang, Y.; Tang, W. M.; Chan, H. L. W. Suppressing the Coffee-Ring Effect in Semitransparent MnO2 Film for a High-Performance Solar-Powered Energy Storage Window. *ACS Appl. Mater. Interfaces* **2016**, *8*, 9088−9096.

(22) Yu, W.; Jia, X.; Long, Y.; Shen, L.; Liu, Y.; Guo, W.; Ruan, S. Highly Efficient Semitransparent Polymer Solar Cells with Color Rendering Index Approaching 100 Using One-Dimensional Photonic Crystal. *ACS Appl. Mater. Interfaces* **2015**, *7*, 9920−9928.

(23) Baetens, R.; Jelle, B. P.; Gustavsen, A. Properties, Requirements and Possibilities of Smart Windows for Dynamic Daylight and Solar Energy Control in Buildings: A State-of-the-Art Review. *Sol. Energy Mater. Sol. Cells* **2010**, *94*, 87−105.

(24) Piccolo, A. Thermal Performance of an Electrochromic Smart Window Tested in an Environmental Test Cell. *Energy Build* **2010**, *42*, 1409−1417.

(25) Wang, J.; Zhang, L.; Yu, L.; Jiao, Z.; Xie, H.; Lou, X. W.; Wei Sun, X. A Bi-Functional Device for Self-Powered Electrochromic Window and Self-Rechargeable Transparent Battery Applications. *Nat. Commun.* **2014**, *5*, 4921.

(26) Lampert, C. M. Large-Area Smart Glass and Integrated Photovoltaics. *Sol. Energy Mater. Sol. Cells* **2003**, *76*, 489−499.

DOI: 10.1021/acsphotonics.6b00518
ACS Photonics 2017, 4, 1−7

(27) Yeh, M.-H.; Lin, L.; Yang, P.-K.; Wang, Z. L. Motion-Driven Electrochromic Reactions for Self-Powered Smart Window System. *ACS Nano* **2015**, *9*, 4757−4765.
(28) Gao, Y.; Luo, H.; Zhang, Z.; Kang, L.; Chen, Z.; Du, J.; Kanehira, M.; Cao, C. Nanoceramic VO2 Thermochromic Smart Glass: A Review on Progress in Solution Processing. *Nano Energy* **2012**, *1*, 221−246.
(29) Kim, H.; Kim, Y.; Kim, K. S.; Jeong, H. Y.; Jang, A.-R.; Han, S. H.; Yoon, D. H.; Suh, K. S.; Shin, H. S.; Kim, T.; Yang, W. S. Flexible Thermochromic Window Based on Hybridized VO_2/Graphene. *ACS Nano* **2013**, *7*, 5769−5776.
(30) Zhu, J.; Zhou, Y.; Wang, B.; Zheng, J.; Ji, S.; Yao, H.; Luo, H.; Jin, P. Vanadium Dioxide Nanoparticle-Based Thermochromic Smart Coating: High Luminous Transmittance, Excellent Solar Regulation Efficiency, and Near Room Temperature Phase Transition. *ACS Appl. Mater. Interfaces* **2015**, *7*, 27796−27803.
(31) Kim, Y.; Jung, D.; Jeong, S.; Kim, K.; Choi, W.; Seo, Y. Optical Properties and Optimized Conditions for Polymer Dispersed Liquid Crystal Containing UV Curable Polymer and Nematic Liquid Crystal. *Curr. Appl. Phys.* **2015**, *15*, 292−297.
(32) Park, S.; Hong, J. W. Polymer Dispersed Liquid Crystal Film for Variable-Transparency Glazing. *Thin Solid Films* **2009**, *517*, 3183−3186.
(33) Gardiner, D. J.; Morris, S. M.; Coles, H. J. High-Efficiency Multistable Switchable Glazing Using Smectic A Liquid Crystals. *Sol. Energy Mater. Sol. Cells* **2009**, *93*, 301−306.
(34) Kwon, H.-K.; Lee, K.-T.; Hur, K.; Moon, S. H.; Quasim, M. M.; Wilkinson, T. D.; Han, J.-Y.; Ko, H.; Han, I.-K.; Park, B.; Min, B. K.; Ju, B.-K.; Morris, S. M.; Friend, R. H.; Ko, D.-H. Optically Switchable Smart Windows with Integrated Photovoltaic Devices. *Adv. Energy Mater.* **2015**, *5*, 1401347.
(35) Sekhar, S. C.; Lim Cher Toon, K. On the Study of Energy Performance and Life Cycle Cost of Smart Window. *Energy Build.* **1998**, *28*, 307−316.
(36) Cupelli, D.; Pasquale Nicoletta, F.; Manfredi, S.; Vivacqua, M.; Formoso, P.; De Filpo, G.; Chidichimo, G. Self-Adjusting Smart Windows Based on Polymer-Dispersed Liquid Crystals. *Sol. Energy Mater. Sol. Cells* **2009**, *93*, 2008−2012.
(37) Cannavale, A.; Manca, M.; De Marco, L.; Grisorio, R.; Carallo, S.; Suranna, G. P.; Gigli, G. Photovoltachromic Device with a Micropatterned Bifunctional Counter Electrode. *ACS Appl. Mater. Interfaces* **2014**, *6*, 2415−2422.
(38) Bloisi, F.; Terrecuso, P.; Vicari, L.; Simoni, F. Voltage Controlled Light Transmittance in Polymer Dispersed Liquid Crystals. *Mol. Cryst. Liq. Cryst. Sci. Technol., Sect. A* **1995**, *266*, 229−239.
(39) Doane, J. W.; Vaz, N. A.; Wu, B.-G.; Žumer, S. Field Controlled Light Scattering from Nematic Microdroplets. *Appl. Phys. Lett.* **1986**, *48*, 269−271.
(40) Firehammer, J. A.; Crawford, G. P.; Lawandy, N. M. Voltage-Controlled Lasing Pixels for Projection Display. *Appl. Phys. Lett.* **1998**, *73*, 590−592.
(41) Chiu, T. L.; Chang, W. F.; Wu, C. C.; Lin, C. F.; Lee, J. Y.; Liu, S. W.; Chen, C. T.; Lee, J. H. Tandem Organic Light-Emitting Diode and Organic Photovoltaic Device Inside Polymer Dispersed Liquid Crystal Cell. *J. Disp. Technol.* **2013**, *9*, 787−793.
(42) Hosseinzadeh, H.; Liew, K.; Han, Y.; Mohieddin, N.; Goldthorpe, I. A. Silver Nanowire Transparent Electrodes for Liquid Crystal-Based Smart Windows. *Sol. Energy Mater. Sol. Cells* **2015**, *132*, 337−341.
(43) Joulain, K.; Mulet, J.-P.; Marquier, F.; Carminati, Rè.; Greffet, J.-J. Surface Electromagnetic Waves Thermally Excited: Radiative Heat Transfer, Coherence Properties and Casimir Forces Revisited in the near Field. *Surf. Sci. Rep.* **2005**, *57*, 59−112.
(44) Higgins, D. A. Probing the Mesoscopic Chemical and Physical Properties of Polymer-Dispersed Liquid Crystals. *Adv. Mater.* **2000**, *12*, 251−264.
(45) Ma, D.; Murray, J.; Munday, J. N.Controllable Propulsion by Light—Steering a Solar Sail via Tunable Radiation Pressure. In review
(46) Murray, J.; Munday, J. N. A Generalized Approach to Modeling Absorption and Photocurrent in Solar Cells with Light Scattering Structures. *J. Appl. Phys.* **2016**, *120*, 165304.
(47) Murray, J.; Munday, J. N. Experimental Demonstration and Modeling of the Internal Light Scattering Profile within Solar Cells due to Random Dielectric Scatterers. *J. Appl. Phys.* **2016**, *119*, 23104.
(48) Drzaic, P. S. *Liquid Crystal Dispersions*; World Scientific: Singapore, 1995.
(49) Green, M. A.; Emery, K.; Hishikawa, Y.; Warta, W.; Dunlop, E. D. Solar Cell Efficiency Tables (Version 45). *Prog. Photovoltaics* **2015**, *23*, 1−9.
(50) Matsui, T.; Sai, H.; Suezaki, T.; Matsumoto, M.; Saito, K.; Yoshida, I.; Kondo, M. Development of Highly Stable and Efficient Amorphous Silicon Based Solar Cells. *Proc. 28th EU PVSEC* **2013**, 2213−2217.
(51) Sharpe, L. T.; Stockman, A.; Jagla, W.; Jagle, H. A Luminous Efficiency Function, V*(Lambda), for Daylight Adaptation. *J. Vis.* **2005**, *5*, 3−3.
(52) Vargas, W. E.; Niklasson, G. A. Generalized Method for Evaluating Scattering Parameters Used in Radiativetransfer Models. *J. Opt. Soc. Am. A* **1997**, *14*, 2243−2252.
(53) Drzaic, P. S. Droplet Density, Droplet Size, and Wavelength Effects in PDLC Light Scattering. *Mol. Cryst. Liq. Cryst. Sci. Technol., Sect. A* **1995**, *261*, 383−392.

DOI: 10.1021/acsphotonics.6b00518
ACS Photonics 2017, 4, 1−7